Khulna University Studies Special Issue ICSTEM4IR: 1-7, 2022

ORIGINAL ARTICLE

SCIENCE & ENGINEERING

MODELLING AND NUMERICAL ANALYSIS OF A HIGHLY-EFFICIENT PCF-BASED AMINO ACID SENSOR

Sandipa Biswas[1], Mahbubul Hasan Abdullah[1], S.M. Shahriar Hasan Shawon[1], Etu Podder[1], Md. Bellal Hossain[1], Abdullah Al-Mamun Bulbul[1]*

[1]Electronics and Communication Engineering Discipline, Khulna University, Khulna-9208, Bangladesh

KUS: ICSTEM4IR-22/0012

Manuscript submitted: June 20, 2022 Accepted: September 25, 2022

Abstract

Amino acids not only play a vital role as protein-building constituents in living beings but also have a wide range of applications that include commercial industries such as food additives and flavor enhancers as well as medical sectors to resist numerous disease levels and to treat digestive abscesses, liver ailments, etc. Hence a precise and feasible detection of amino acids is a fervent desire for their appropriate applications. This paper presents an amino acid sensor employing a mono-circular hollow-core PCF. This PCF-based sensor has been designed maintaining high fabrication feasibility. Then the performance of this sensor has been numerically studied engaging finite element method while sensing five types of amino acids. Performance metric exhibits that this sensor has a very low effective material and confinement loss of about 0.003795 cm^{-1} and 3.065×10^{-15} cm^{-1} correspondingly at 2.7 THz for Tryptophan. Besides this sensor has offered approximately 97.12% relative sensitivity maintaining a higher numerical aperture for the same type of amino acid. This sensor has maintained admirable values for all the performance indices for all the five types of amino acids analyzed in this paper. Furthermore, the elementary design of this sensor has opened the door of viable fabrication with the aid of existing sol-gel technique or extrusion with 3D printing method.

Keywords: Amino acids, EML, FEM, relative sensitivity, PCF

Introduction

Proteins which are made up of amino acids play a crucial part in multiple biological functioning such as cell division, hormone, and neurotransmitter production (brain chemicals). So, sensing amino acids is very important in determining the quantity and purity of proteins in a mixture, defining the proportions of amino acids, validating known proteins in databases, and the identification of novel protein particles.

To sense different analytes (liquids/gases), researchers have developed several techniques during the past few decades (Hoo et al., 2001; Kiwa et al., 2008). Micro-structured PCFs are useful for sensing solutions (Cordeiro et al., 2006; Monro et al., 2001). Several PCF models that operate in the optical wavelength have recently been developed for chemical sensing (Ademgil & Haxha, 2015; Kaur & Singh, 2017; Otupiri et al., 2014). So far numerous PCF sensors have been developed for sensing various chemicals. Researchers have focused to polish up the sensing parameters like the effective area (EA), confinement loss (CL), and effective material loss (EML) with high power fraction (PF) and relative sensitivity (RS) in a THz frequency region (Islam et al., 2017; Sultana et al.,

*Corresponding author: <bulbul@ku.ac.bd>

DOI: https://doi.org/10.53808/KUS.2022.ICSTEM4IR.0012-se

2018). In recent times, researchers developed a PCF model which was operated at 1.81 THz to sense Bane Chemicals (Hossain et al., 2020). They received a high PF of 94.40% and low CL of about 1.70×10^{-14} cm^{-1} and an EML of 0.009 cm^{-1}. So, it is clear that researchers are always striving to improve the efficiency of PCF-based chemical sensors operating in the THz range. In this paper, we have developed a PCF sensor model that can sense various kinds of amino acids in real-time with comparatively better optical parameters.

Model Design

Finite element method (FEM) based software platform is utilized to model and simulate the proposed PCF-based sensor. The medium of the suggested model has been homogenized using full vector FEM. Furthermore, the full vector FEM was also used to analyze the model's effective material characteristics. A sectional outlook of our PCF sensor is shown in Figure 1. The core of this model is the indigo-colored central circle, which is surrounded by air. The core radius is 175 µm while the radius of the model is 950 µm with 76 µm of PML. The width of the cladding air region is 20.5 µm with 13 µm of strut.

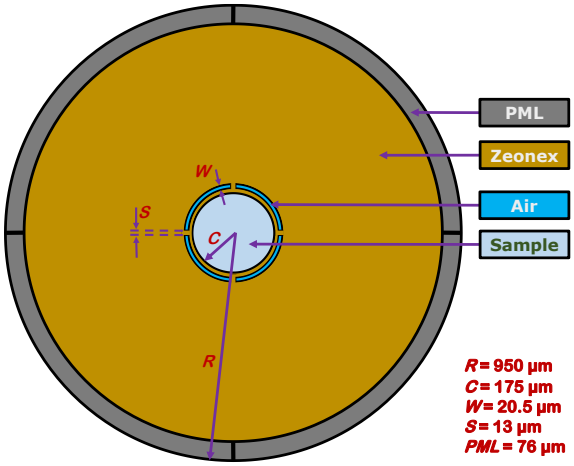

Figure 1. Sectional outlook of the anticipated PCF sensor.

Zeonex has been used as the fundamental fiber material in this case. It was chosen over topaz, silicon, and other materials due to its reduced terahertz absorption loss and a bulk material loss of 0.2 cm^{-1} in the terahertz region (0.1-10 THz) while maintaining an almost constant RI (1.53) (Islam et al., 2017; Sultana et al., 2018). Furthermore, it exhibits lower values for material absorption-loss and dispersion, as well as greater values for transparency, humidity insensitivity, and temperature insensitivity. These characteristics make it ideal for chemical detection in the THz range.

With existing manufacturing technology, there have been a variety of fabrication procedures developed, each of which is best suited to particular PCF architectures. Our PCF model is symmetrical in shape, with one circular section at the core with four air slots of equal arc size. Stack and draw (Broeng et al., 1999), drilling (Lee et al., 1988), and the sol-gel process (El Hamzaoui et al., 2012) are some of the most prevalent manufacturing methods. Extrusion, when paired with 3D printing, allows for the fabrication of complicated shapes and patterns, as well as huge air filling fractions. Because capillary stacking is not required, there are fewer contacts required, resulting in minuscule losses. It is also quite economical. As a result, extrusion is the best method for constructing the suggested PCF sensor model.

Materials and Methods

Different amino acids were introduced as analytes into the sensor and multiple simulations were run for them. Optical parameters such as EA, EML, CL, PF, RS, and numerical aperture (NA) are all measured studying the light

properties inside the proposed PCF at each time.

EML results from the light captivation by the background material chosen in the PCF design. Low EML is required for better sensing and the usage of the porous core to minimize EML might play a good role, as greater porosity reduces the proportion of fiber material. The following equation (2) is used to calculate the EML for our designed PCF.

$$\alpha_{eff} = \left(\frac{\varepsilon_0}{\mu_0}\right)^{\frac{1}{2}} \frac{\int_{\text{mat}} n_{mat}|E|^2 \alpha_{mat} dA}{2\int_{\text{all}} S_z dA},\ \text{cm}^{-1} \tag{1}$$

Here, α_{eff} is the EML, ε_0 represents Free-space permittivity, μ_0 represents free-space permeability, n_{mat} defines Zeonex's RI, E stands for electric field, α_{mat} is the loss due to the absorption of Zeonex, and S_z denotes the z-component of Poynting vector.

CL occurs due to an insufficient structure in the PCF cladding area, and the increase of hollow area in this zone can help to reduce CL. The following equation (3) can be used to express it.

$$\alpha_{cl} = \left(\frac{4\pi f}{c}\right) \text{Im}\left(n_{eff}\right), cm^{-1} \tag{2}$$

Here, α_{cl}, $\text{Im}\left(n_{eff}\right)$, and *f* are the CL of the anticipated sensor, imaginary portion of the effective RI, and frequency respectively.

Sensitivity is a measurement of the dealings between the entire amount of light traveling through the core and the amount of light passing through the cladding. This numerical value describes a PCF's ability to detect certain analytes introduced into the core area. Equation (4) is used to calculate the sensitivity.

$$R = \frac{n_{mat}}{n_{eff}} \times P_f\% \tag{3}$$

Here, n_{mat} is the fiber material's RI, n_{eff} is the Effective RI of the PCF, and P_f is the power fraction.

$$P_f = \frac{\int_{\text{Sample}} R_e\left(E_x H_y - E_y H_x\right) dxdy}{\int_{\text{Total}} R_e\left(E_x H_y - E_y H_x\right) dxdy} \times 100 \tag{4}$$

The EA, which is calculated using Equation, is the region contained by the mode field within the central region of the fiber.

$$A_{eff} = \frac{\left[\int I(r) r dr\right]^2}{\left[\int I^2(r) dr\right]} \tag{5}$$

Here, $I(r) = |E_t|^2$ defines the strength of the electric field in the PCF.

The numerical aperture may actualize the quantity of collected power in the core of a PCF, and it is dependent on the EA of the proposed PCF. Following equation helps in computing the numerical aperture (N_A) of the proposed sensor.

$$N_A = \frac{1}{\sqrt{1 + \frac{\pi A_{eff}}{\lambda^2}}} \tag{6}$$

Here, λ stands for the wavelength of light.

Results

Figure 2 shows the fundamental mode field scheme for tryptophan analyte at a frequency of 2.70 THz. The core light intensity is the strongest and progressively decreases throughout the radius of the PCF, displaying a Gaussian profile, as visible in the picture. It can also be observed that light is hermetically contained inside the hollow core area, causing the suggested fiber to establish a strong interaction between field and sensing substance. As a result, the RS of our suggested sensor fiber will be high.

(a) *x*-Pol (b) *y*-Pol

Figure 2. Fundamental mode field scheme for the modelled sensor while sensing tryptophan.

Table 1. Core Radius (CR) Comparison (Tryptophan)

Model	Frequency	EA in *x*-Pol (μm^2)	NA in *x*-Pol	EML in *x*-Pol (cm^{-1})	RS in *x*-Pol (%)
CR: 150 μm	2.7 THz	51056	0.2673	0.003924	96.1216
CR: 175 μm	2.7 THz	67712	0.2342	0.003795	97.1154
CR: 200 μm	2.7 THz	86830	0.2081	0.003756	97.8264

First, we selected our optimum model by using the trial-and-error method adjusting the radius of the core and cladding width at different times. We tuned the core keeping the cladding width of 20.5 μm constant. Then we measured various optical parameters and find out that with a 175 μm core radius the PCF shows the overall best performance which is shown in Table 1. A slightly higher RS is found for 200 μm CR compared to 175 μm CR, but NA is lower than 0.23, as well as, EA is comparatively higher for this case. Hence we have selected 175 μm as the CR. Then we tuned the width of the cladding keeping the core radius constant at 175 μm. Again we measured different optical parameters and find out that with a 20.5 μm cladding width the PCF shows the overall best performance which is shown in Table 2. We have started the simulation from 0 μm, i.e., no cladding, to 150.5 μm cladding width with little incremental value less than equal 5.125 μm. Each time we have studied the performance indices. However, we haven't presented all the results in the table as all of them didn't exhibit significance differences. As the modelled sensor is circular shaped, no noteworthy difference has been noticed between the *x*-polarization (Pol) and *y*-Pol mode. Hence, we have presented the results for the *x*-Pol only.

Table 2**.** Cladding (i.e., Air) Width (AW) Comparison (simulated results for Tryptophan)

Model	Frequency	EA in *x*-Pol (μm^2)	NA in *x*-Pol	EML in *x*-Pol (cm^{-1})	RS in *x*-Pol (%)
AW: 0 μm	2.7 THz	71043	0.2289	0.0081899	94.1689
AW: 20.5 μm	2.7 THz	67712	0.2342	0.003795	97.1154
AW: 150.5 μm	2.7 THz	68519	0.2329	0.004297	97.6026

The EA in the *x*-Pol of the modelled sensor is presented in Fig. 3(a), where the curve follows a diminishing incurvate pattern. This is because high frequency light usually remains further restricted in the core, reducing the

DOI: https://doi.org/10.53808/KUS.2022.ICSTEM4IR.0012-se

EA. Fig. 3(b) shows a graph of the numerical aperture *vs* operating frequency in the *x*-Pol. The numerical aperture is heavily dependent on the EA. The NAs of the sensor are nearly the same for all analytes. Fig. 3(c) shows how EML varies in *x*-Pol with operation frequency. The EML rises with increased frequency, as seen in Figure. Fig. 3(d) depicts a plot of CL against frequency in *x*-Pol, which indicates that the CL decreases at a fluctuating rate as the mode field becomes more contained at the core at high frequencies. Fig. 3(e) depicts a comparative examination of the RS in *x*-Pol for the five different amino acids, demonstrating that when the operating frequency is increased, the sensitivity steadily increases. The numerical results for different optical parameters while detecting different amino acids employing the proposed sensor are presented in Table 3. Besides, Table 4 shows a differentiation of the modelled sensor with a few earlier PCF sensors.

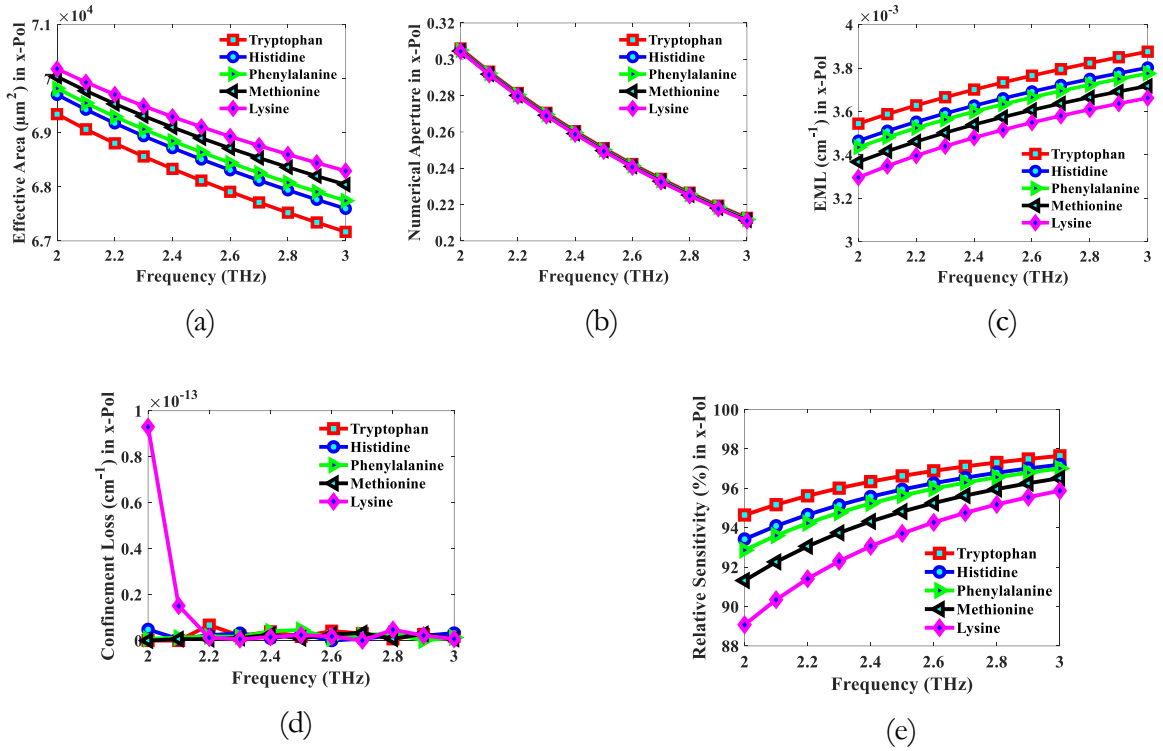

Figure 3. Performance indices of the modelled sensor while sensing different amino acids.

Table 3. Numerical values of performance indices of the modelled sensor for different amino acids

Analytes	EA (μm^2)	NA	EML (cm^{-1})	CL (cm^{-1})	RS (%)
Tryptophan	67712	0.2342	0.003795	3.065×10^{-15}	97.1154
Histidine	68120	0.2335	0.003721	7.96×10^{-16}	96.5425
Phenylalanine	68259	0.2333	0.003695	2.42×10^{-15}	96.2922
Methionine	68535	0.2329	0.003637	3.291×10^{-15}	95.6358
Lysine	68762	0.2325	0.00358	0	94.7595

Table 4. Differentiation between the previous PCF sensors and the anticipated sensor

Analytes	Frequency (THz)	EA (μm^2)	EML (cm^{-1})	CL (cm^{-1})	RS (%)
Spectroscopic Chemical (Islam et al., 2017)	1.60	69806	-	-	85.69
Alcohol (Sultana et al., 2018)	1.01	-	0.05	8.00×10^{-12}	68.86
HCN (Islam et al., 2018)	1.78	-	-	5.14×10^{-8}	77.52
Bane Chemicals (Hossain et al., 2020)	1.81	-	.009	1.70×10^{-14}	94.40
Tryptophan [Proposed]	2.7	67712	0.0038	3.07×10^{-15}	97.12

Conclusion

The suggested PCF sensor model has a lot of optical parameter flexibility and good sensing performance for sensing and categorizing amino acids. The RS for amino acids sensing and classification is 97.11% for Tryptophan, 96.54% for Histidine, 96.29% for Phenylalanine, 95.63% for Methionine and 94.75% for Lysine in the *x*-Pol. In Table 4, there is showing an association between the previous PCF sensors and the modelled sensor which indicates that our suggested model outperforms among them and provides a better sensing performance. So, it seems obvious that the modelled sensor might play essential functions in the areas of biosensing.

References

Ademgil, H., & Haxha, S. (2015). PCF based sensor with high sensitivity, high birefringence and low confinement losses for liquid analyte sensing applications. *Sensors*, *15*(12), 31833-31842.

Broeng, J., Mogilevstev, D., Barkou, S. E., & Bjarklev, A. (1999). Photonic crystal fibers: A new class of optical waveguides. *Optical Fiber Technology*, *5*(3), 305-330.

Cordeiro, C. M., Franco, M. A., Chesini, G., Barretto, E. C., Lwin, R., Cruz, C. B., & Large, M. C. (2006). Microstructured-core optical fibre for evanescent sensing applications. *Optics express*, *14*(26), 13056-13066.

El Hamzaoui, H., Ouerdane, Y., Bigot, L., Bouwmans, G., Capoen, B., Boukenter, A., . . . Bouazaoui, M. (2012). Sol-gel derived ionic copper-doped microstructured optical fiber: a potential selective ultraviolet radiation dosimeter. *Optics express*, *20*(28), 29751-29760.

Hoo, Y., Jin, W., Ho, H. L., Wang, D., & Windele, R. S. (2001). Evanescent wave gas sensing using microstructure fibre. Technical Digest. CLEO/Pacific Rim 2001. 4th Pacific Rim Conference on Lasers and Electro-Optics (Cat. No. 01TH8557),

Hossain, M. B., Podder, E., Bulbul, A. A.-M., & Mondal, H. S. (2020). Bane chemicals detection through photonic crystal fiber in THz regime. *Optical Fiber Technology*, *54*, 102102.

Islam, M. S., Sultana, J., Ahmed, K., Islam, M. R., Dinovitser, A., Ng, B. W.-H., & Abbott, D. (2017). A novel approach for spectroscopic chemical identification using photonic crystal fiber in the terahertz regime. *IEEE Sensors Journal*, *18*(2), 575-582.

Islam, M. S., Sultana, J., Dinovitser, A., Faisal, M., Islam, M. R., Ng, B. W.-H., & Abbott, D. (2018). Zeonex-based asymmetrical terahertz photonic crystal fiber for multichannel communication and polarization maintaining applications. *Applied optics*, *57*(4), 666-672.

Kaur, V., & Singh, S. (2017). Extremely sensitive multiple sensing ring PCF sensor for lower indexed chemical detection. *Sensing and Bio-Sensing Research*, *15*, 12-16.

Kiwa, T., Kondo, J., Oka, S., Kawayama, I., Yamada, H., Tonouchi, M., & Tsukada, K. (2008). Chemical sensing plate with a laser-terahertz monitoring system. *Applied optics*, *47*(18), 3324-3327.

Lee, C., Yang, W., & Parr, R. G. (1988). Development of the Colle-Salvetti correlation-energy formula into a functional of the electron density. *Physical review B*, *37*(2), 785.

Monro, T. M., Belardi, W., Furusawa, K., Baggett, J. C., Broderick, N., & Richardson, D. (2001). Sensing with microstructured optical fibres. *Measurement Science and Technology*, *12*(7), 854.

Otupiri, R., Akowuah, E. K., Haxha, S., Ademgil, H., AbdelMalek, F., & Aggoun, A. (2014). A novel birefrigent photonic crystal fiber surface plasmon resonance biosensor. *IEEE Photonics Journal*, *6*(4), 1-11.

Sultana, J., Islam, M. S., Ahmed, K., Dinovitser, A., Ng, B. W.-H., & Abbott, D. (2018). Terahertz detection of alcohol using a photonic crystal fiber sensor. *Applied optics*, *57*(10), 2426-2433.